Theoretical and Experimental Cryobiology

https://doi.org/10.15407/cryo36.02.095
UDC: 577.352.5:576.5: 57.086.13

Olga I. Gordiyenko*, Yevgeniya I. Smolyaninova, Hanna L. Poliakova, Svitlana Ye. Kovalenko, Igor F. Kovalenko, Oleksandr F. Todrin
Institute for Problems of Cryobiology and Cryomedicine of the National Academy of Sciences of Ukraine, Kharkiv, Ukraine
*olga.gordiyenko.ipcic@gmail.com

DISTRIBUTION BY TRANSMEMBRANE POTENTIAL OF L929 CELLS IN SUSPENSION BEFORE AND AFTER FREEZING

Monitoring of cell membrane potential is an important tool for assessing their state during functioning, as well as under the influence of external factors. The distribution of transmembrane potential of L929 cells in cultured suspension and after freezing is determined in this work. It is shown that in the control suspension, cells are in different phases of the cell cycle: a larger fraction of cells (82%) is in a hyperpolarized state of varying degrees (G1 and S-phases), and only a small percentage of them (~7%) are in the division stage and have a low transmembrane potential value (depolarized cells). Freezing the L929 cell suspension in the standard mode (10% DMSO, cooling rate of 1 °C/min to –80 °C with subsequent immersion in liquid nitrogen) practically does not change the part of cells in the hyperpolarized state. At the same time, the fraction of cells in the depolarized state disappears. Obviously, cells that were in the division stage are more sensitive to cryodamage factors. Freezing a suspension of L929 cells with a reduced concentration of DMSO (5%) resulted in a significant decrease in the part of cells in a hyperpolarized state and a significant decrease in the ability of cells to adhere.

Key words: *L929 cells, transmembrane potential, cell cycle, adhesion, freezing.*

The transmembrane potential (V_{mem}) is a fundamental biophysical parameter present in all cells. It is the result of differences in ion concentration across a semipermeable membrane. Therefore, any disruption of the permeability of the cell plasma membrane or the mechanisms of active ion transport will cause deviations of V_{mem} from the value characteristic of a given cell type. That is, Vmem is inherently a system-level property determined by the structure of the membrane and the set of ion channels and pumps. Therefore, monitoring the cell membrane potential is an important tool for determining their state during functioning, as well as under the influence of external factors.

The first studies of V_{mem} were carried out on large cells (giant algae cells, giant squid axons, muscle cells) using intracellular glass microelectrodes. With the improvement of the measurement technique, the use of ultrathin microcapillaries was extended to a variety of small cells, in particular isolated cultured cells. Based on these studies, it was concluded that cells that are electrically excitable are characterized by high V_{mem} in the resting state, while small non-excitable cells have low V_{mem}. However, evidence began to emerge that measurements made using distribution indicators gave high V_{mem}, while electrodes showed low values [30]. It turned out that when studying small cells using the microcapillary technique, there is a problem of sealing and leakage of cations through the membrane-glass sealing layer [20].

Reference: Gordiyenko OI, Smolyaninova YI, Poliakova HL, Kovalenko SYe, Kovalenko IF, Todrin OF. Distribution by transmembrane potential of L929 cells in suspension before and after freezing. *Probl Cryobiol Cryomed*. 2026; 36(2): 95—105. https://doi.org/10.15407/cryo36.02.095

A significant improvement in the technique for determining V_{mem} in small cells was provided by the advent of so-called patch-electrodes [19], which were tightly attached to the outside of cell membranes and could be sealed with a resistance of up to 10^{11} Ω, compared to less than $5 \cdot 10^9$ Ω for penetrating electrodes. The whole-cell patch-electrode technique was applied to mouse embryonic fibroblasts (L cells) cultured in suspension [20]. The authors obtained V_{mem} in the range of –50 to –75 mV, whereas previous studies reported –15...–20 mV. These results suggest that previous reports of resting V_{mem} in small cultured cells should be revised. In the authors' opinion, the highest values (around –75 mV) are the best estimates of the true resting V_{mem} in L cells.

The appearance of optical methods for measuring V_{mem} [13] has opened up new possibilities for studying V_{mem} in small, non-excitable cells. The first attempts to determine absolute values of V_{mem} using fluorescent potential-dependent probes were based on simultaneous electrophy-siological measurements with glass microelectrodes and the fluorescence intensity of the probe in a single cell [11]. However, as already noted, this approach introduces significant errors in determining the relationship between fluorescence intensity and absolute value of V_{mem} [30]. These problems were solved using patch-electrodes [19]. However, the use of difficult methods for measuring V_{mem} using microelectrodes for calibrating the fluorescence intensity of potential-dependent probes negates the advantages of their use and does not provide guaranteed measurement accuracy. Therefore, when measuring V_{mem} with fluorescent indicators, the relative changes were taken, and not the absolute values of the measured parameter. As a prerequisite for determining absolute values, a calibration curve is mandatory to establish a definite relationship between fluorescence and transmembrane potential. Approaches that use a series of different isoosmotic compositions of the external buffer and the addition of an appropriate ionophore (usually valinomycin or gramicidin, depending on whether a cationic or anionic dye is used) to give a specific change in V_{mem} based on the Nernst potential for extra- and intracellular sodium and potassium cations are less laborious and also well-established [5, 12, 15, 25, 26, 29, 34, 46]. However, to simplify the procedure, intracellular cation concentrations have usually only been estimated [5, 25, 26, 29, 46] rather than actually measured. Furthermore, even for the most well-studied cells, such as erythrocytes, the intracellular concen-trations of major ions vary from author to author [3, 4, 31, 36, 41, 44], which affects the calculated values of V_{mem}.

In this regard, the method proposed by Krasznai *et al.* [27] has the advantage that intracellular cations do not need to be taken into account for calibration. In this work, a protocol is proposed for measuring V_{mem} on an absolute scale using the dye bis(1,3-dibutylbarbituric acid(5)) trimethine oxonol (diBA-C4-(3)). This method is based on the assumption that, due to their net negative charge, diBA-C4-(3) molecules distribute across the cytoplasmic membrane according to the Nernst equation. The intracellular concentration of the dye is calculated based on its concentration and the fluorescence of cells fully depolarized with paraformaldehyde, [6, 27], methanol [43], or gramicidin [38].

The aim of the study was to determine the absolute values of transmembrane potentials of L929 cells in cultured suspension and the influence of freezing conditions on this parameter.

MATERIALS AND METHODS

Reagents. Dimethyl sulfoxide — (≥99.7%, HybriMax(TM), filter-sterilized (Sigma-Aldrich, Germany); dye bis(1,3-dibutylbarbituric acid(5)) trimethinoxonol (diBA-C4-(3)), ≥95%, (Sigma-Aldrich); Gramicidin A from *Bacillus brevis* (Sigma-Aldrich).

The dye was dissolved in DMSO and stored as a concentrated solution (22 mM) at –20 °C in the dark. Fresh dilutions of the stock solution were prepared for each experiment. Aliquots of the pre-diluted dye solutions were added either directly or after further dilution to the cell suspensions to obtain the desired final dye concentration.

Gramicidin used to depolarize cells was dissolved in DMSO at a concentration of 2 mg/ml. Cells were exposed to gramicidin at a concentration of 2 μg/mL. Measurements were performed 30 minutes after exposure to gramicidin and dye. During incubation, cells were maintained at 37 °C in tubes covered with aluminium foil.

Cells. The studies were performed on the L929 cell line, which was obtained from a cryopreserved culture stored at –196 °C in the cryobank of the Institute for Problems of Cryobiology and Cryomedicine of the NAS of Ukraine. The cells were

cultured in DMEM/F12 medium (Biowest, France) containing 200 U/mL benzylpenicillin (Arterium, Ukraine), 200 μg/mL streptomycin (Arterium), and 10% fetal calf serum (Biowest) at 37 °C in an atmosphere of 5% CO_2 in plastic culture bottles (SPL Life Sciences, Korea). The seeding concentration of cells to obtain the initial culture was 2 × × 10^5 cells/mL.

Cell cryopreservation. For cryopreservation, a monolayer cell culture of 5—7 days of cultivation was used. The cell monolayer was detached from the surface of the culture flask by sequential treatment for 2 min with Versene solution (Vetline, Ukraine) and 0.25% trypsin solution (Biowest, France) for 10 min. Then the cells were washed from the enzymatic solution by centrifugation in DMEM/F12 medium with the addition of 10% FCS at 1500 rpm for 3 min in an MPW-260R centrifuge (MPW Med. Instruments, Poland). The pellet was resuspended in 0.5 mL of DMEM/F12 nutrient medium and an equal volume of the appropriate cryoprotective medium with double concentration of cryoprotectant and FCS was added. Each cryotube was filled with 1 mL of cell suspension with a concentration of 10^6 cells/mL. DMSO with a concentration of 10% (vol/vol) was used for cryopreservation. In addition, cells that were frozen with a reduced amount of DMSO (5%) were studied. Cryopreservation was performed using cryovials (Nunc, USA). Freezing was performed at a cooling rate of 1 °C/min to –80 °C with subsequent immersion in liquid nitrogen (standard mode).

Cell warming. The samples were warmed in a water bath at 37 °C until the solid phase disappeared. To remove the cryoprotectant, 10 times the volume of culture medium was added to the cell suspension, centrifuged for 5 min at 1200 rpm, and the supernatant was removed. This procedure was repeated twice. The cell suspension pellet obtained after warming and removal of the cryoprotectant was resuspended in 1 mL of culture medium, after which cell counting was performed.

The fluorescence intensity values of cells were measured using a LSM 510 META confocal microscope (Carl Zeiss, Germany). In the control suspension, fluorescence was measured and the V_{mem} value calculated for 140 cells, in the suspensions after freezing — for 90 cells.

To study adhesion, cells were plated on a glass substrate measuring 25.4 mm × 25.4 mm × 1 mm at a concentration of 3—4 × 10^5 cells/mL.

Theoretical justification of the fluorescence calibration method. According to the protocol described in [18, 27], due to the total negative charge, diBA-C4-(3) molecules are distributed through the cytoplasmic membrane according to the Nernst equation. Since the dye is a monovalent anion, it can be written

$$V_{mem} = RT/F[\ln(D_i/D_e)] \quad (1)$$

where R is the universal gas constant, T — the absolute temperature, F — the Faraday constant, and D_i and D_e are the intra- and extracellular concentrations of free dye, respectively.

Therefore, determining the absolute value of V_{mem} is a matter of determining the ratio of the free dye concentrations on both sides of the cytoplasmic membrane D_i/D_e. To determine this ratio, the concentration dependence of the fluorescence intensity of the studied cells stained with diBA-C4-(3) (between 100 nM and 2 μM) in suspension is obtained. The calibration curve displays the average values of the measured cellular fluorescence as a function of the extracellular concentration of the dye. Due to the relationship between the extracellular and intracellular concentrations of the free dye and the V_{mem} of the cells (1) used to construct the calibration curve, the abscissa of this plot can be further scaled in terms of D_i as

$$D_i = D_e \exp(FV_{mem}/RT) = D_eC, \quad (2)$$

where C is a constant at a constant value of V_{mem}.

The transmembrane potential of the sample under study can be calculated from the ratio D_i^S/D_e^S using the Nernst equation (1) (the superscript S refers to the sample under study). For the calculation, data from a sample with fully depolarized (but otherwise identical to those used in the experiment) cells are used. Instead of defining D_e^S, we define D_i^0 ($D_e^S = D_i^0$), where the superscript 0 refers to a sample with fully depolarized cells (with $V_{mem} = 0$) stained in the presence of exactly the same concentration of dye as the sample of interest. The results obtained using the Krasznai method [27] were found to be consistent with data obtained using patch-electrode measurements on whole cells.

RESULTS

Construction of a calibration curve for determining the transmembrane potential of L929 cells. Cells were suspended at a concentration of 10^5 ml^{-1} in PBS containing different concentrations of dye.

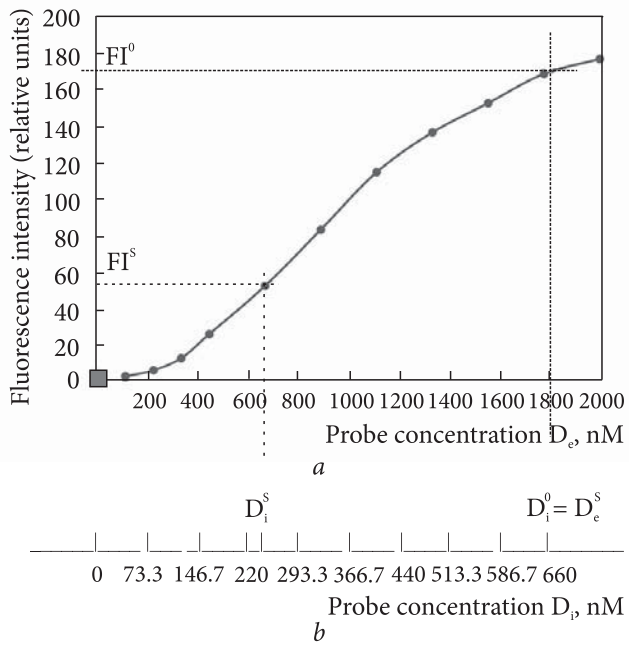

Fig. 1. Average fluorescence intensity of L929 cells stained with different concentrations of the membrane potential indicator diBA-C4-(3). Extracellular (D_e^S — *a*) and intracellular (D_i^S — *b*) concentrations of the membrane potential indicator dye. The superscripts S and 0 refer to the measured sample and depolarized cells, respectively

Table 1. **Calculated values of intracellular probe concentrations and transmembrane potentials for different fluorescence levels**

Fluorescence intensity, rel. un.	D_i^S, nM	C^S	Transmembrane potential V_{mem}, mV
1	33.0	0.05	−75.6
4	66.0	0.10	−58.1
5	73.3	0.11	−55.5
16	135.6	0.20	−40.0
17	139.3	0.21	−39.3
20	146.6	0.22	−38.0
33	186.9	0.28	−31.8
39	205.2	0.31	−29.5
42	212.6	0.32	−28.6
49	238.2	0.36	−25.7
53	249.2	0.38	−24.6
76	307.8	0.46	−19.2

The dependence of the fluorescence intensity of cells on the concentration of the probe in the extracellular solution $[diBA-C4-(3)]_e$ is shown in Fig. 1*a*.

Since increasing the dye concentration does not affect V_{mem}, the abscissa of the plot can be changed in terms of D_i, (Fig. 1*b*). According to the assumptions made, the measured fluorescence intensity is a well-defined function of D_i. Furthermore, D_i is the only variable that affects the detected emission intensity for a given cell (with a given membrane potential) under the same microscope settings. This allows us to use the plot of cell fluorescence intensity versus extracellular probe concentration (Fig. 1*a*) as a generally accepted calibration curve and calculate Di from fluores-cence readings on a relative scale (Fig. 1*b*).

Using the graph of the dependence of the fluorescence intensity of L929 cells on the probe concentration in the extracellular medium (Fig. 1*a*) and the fluorescence value of depolarized L929 cells at a probe concentration of 660 nM (FI^0 = 169 rel. units, Fig. 1*a*, Fig. 2), we determine the corresponding scale of intracellular dye concentrations (Fig. 1*a*) and calculate the V_{mem} of cells from the fluorescence intensity at the same probe concentration according to the formula (1). Taking into account the value and dimension of the constants (R, F) and the absolute temperature T {R = = 8.31 J/mol × K, F = 96485.33 C/mol, T = 293 K (20 °C)}, we obtain RT/F = 0.025. The calculated values of transmembrane potentials for different fluorescence levels are presented in Table 1.

Determination of transmembrane potential of L929 cells. For the population of native cells (cells after recultivation), the following results were obtained. The V_{mem} values of the main part of cells (54.5%) ranged from −75 to −58 mV; 27.5% of cells had potentials from −55 to −40 mV; 4.3% of cells — from −39 to −30 mV; 6.5% of cells — from −29 to −25 mV and 7.2% of cells had potentials from −24 to −20 mV (Tabl. 2, Figs 3, 4). Thus, the main fraction of cells in the native cell suspension has a high V_{mem} of −75...−58 mV. However, there is a small proportion of cells (~14%) that has a relatively low V_{mem} (< −30 mV).

In the suspension frozen with 10% DMSO immediately after thawing, the fraction of cells with low V_{mem} (< −30 mV) disappears. Apparently, cells with low V_{mem} die during freezing. At the same time, the number of cells with V_{mem} from −55 to −40 mV (34.5%) and from −39 to −30 mV (14.5%) increases, and the part of cells with high V_{mem} (−75...−58 mV) remains quite high (51% compared to 54.5% in the native suspension) (Figs 5, 6). After freezing the cell suspension with 5% DMSO,

the number of cells with high V_{mem} de-creases to 36% and the fraction of cells with V_{mem} less than –40 mV increases to 35% (Figs 7, 8).

The effect of freezing on the adhesion and proliferation capacity of L929 cells. Cells that were frozen under the optimal regime (10% DMSO, cooling rate of 1 °C/min to –80 °C with subsequent immersion in liquid nitrogen) create a full-fledged monolayer one day after seeding and occupy almost the entire area of the substrate, and on the second day they occupy the entire area. On the third day, a second layer of cells begins to grow (Fig. 9*a*, *b*, *c*). Cells that were frozen with 5% DMSO did not create a monolayer (Fig. 9*d*, *e*, *f*). On the first day after seeding, the cells are highly sparse and occupy a small area of the substrate surface. Obviously, this is due to the fact that after freezing in suboptimal conditions, a smaller part of viable cells remains. This is con-sistent with the data on the distribution of cells by V_{mem} after thawing (Fig. 8). On the second and third day, viable cells begin to divide and gradually fill the area of the substrate.

DISCUSSION

Studies of V_{mem} in small, quiescent cells have shown that the resting potentials of different cell types lie in a wide range (from –10 to –90 mV), and the position of cells along this V_{mem} scale usually corresponds to their proliferative potential [8, 45]. The first correlations between V_{mem} and proliferative capacity arose from the observation that cells with very high resting V_{mem}, such as muscle cells and neurons, show little or no mitotic activity [9]. V_{mem} oscillations occurring during cell cycle progression have been shown in Chinese hamster lung cells [7]. During the G0/G1 transition, V_{mem} gradually shifts from an intermediate depolarization state to an intermediate hyperpolarization state. As the cell passes through the G1/S

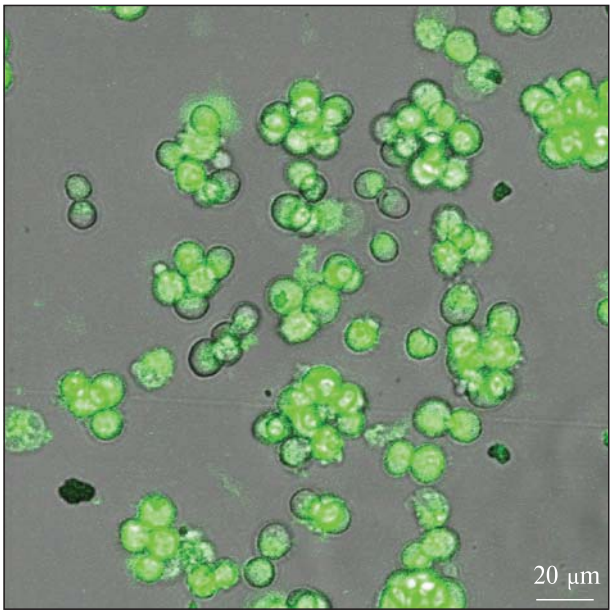

Fig. 2. Fluorescence of the probe diBA-C4-(3) in depolarized L929 cells at a probe concentration in suspension of 660 nM. The measured fluorescence intensity FI^0 = 169 rel. units

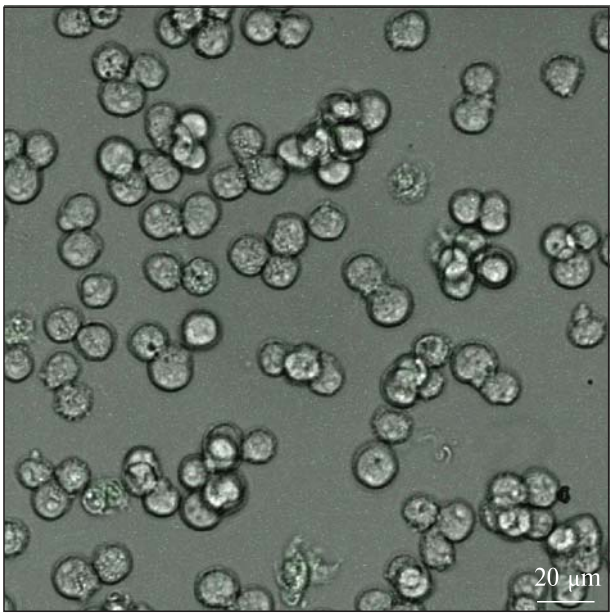

Fig. 3. Fluorescence of the diBA-C4-(3) probe in control L929 cells at a probe concentration in suspension of 660 nM

Table 2. **Distribution of cells by transmembrane potential in L929 cell suspension**

Potential range, mV	Cell portion, %		
	Control suspension	After freezing with 10% DMSO	After freezing with 5% DMSO
–75…–58	54.5	51	36.5
–55…–40	27.5	34.5	28.5
–39…–30	4.3	14.5	35
–29…–25	6.5	—	—
–24…–20	7.2	—	—

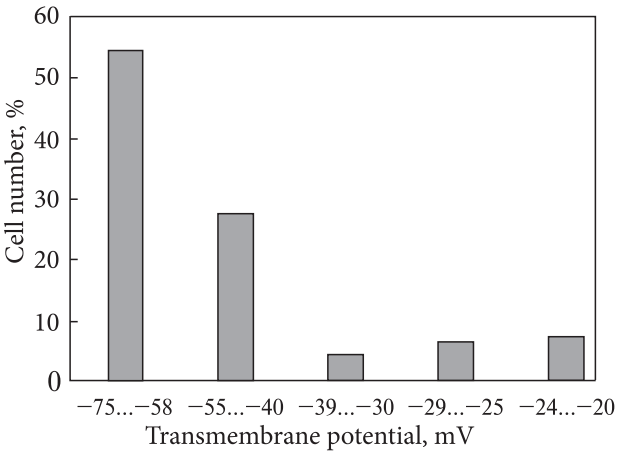

Fig. 4. Distribution of L929 cells by transmembrane potential in native suspension

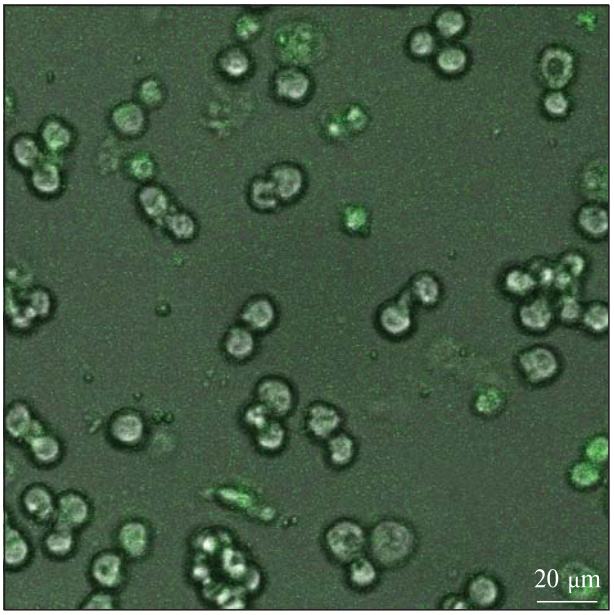

Fig. 5. Fluorescence of the diBA-C4-(3) probe in L929 cells frozen with 10% DMSO at a probe concentration in suspension of 660 nM

phase transition checkpoint, V_{mem} becomes even more negative, indicating hyperpolarization of the cell membrane. During the transition through S-phase, the S/G2 checkpoint, and G2-phase, the membrane potential has a maximum negative value and remains hyperpolarized. Upon entering mitosis, V_{mem} rapidly depolarizes to a lower minimum value, indicating the completion of cell division. In [16, 32], it was shown that rat bone marrow MSCs have variable membrane potentials from −15 to −55 mV. V_{mem} was −41.3 mV in early G1 phase, increased to −48.6 mV in cells progressing through G1 phase, and to −52.2 mV in late G1

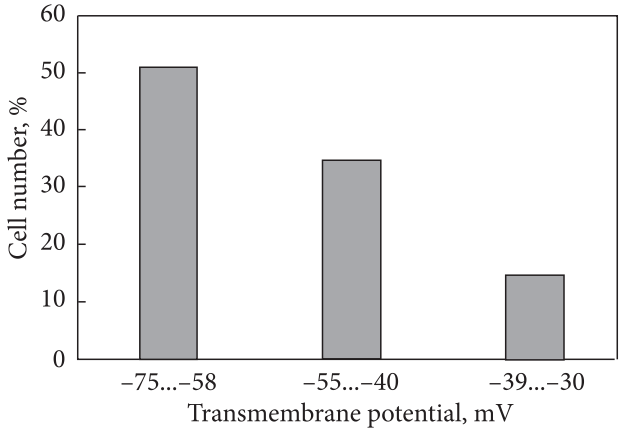

Fig. 6. Distribution of L929 cells by transmembrane potential in suspension after freezing with 10% DMSO

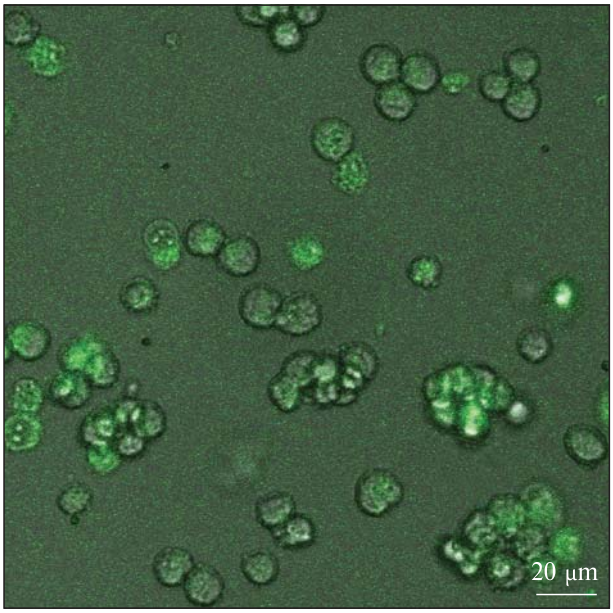

Fig. 7. Fluorescence of the diBA-C4-(3) probe in L929 cells frozen with 5% DMSO at a probe concentration in suspension of 660 nM

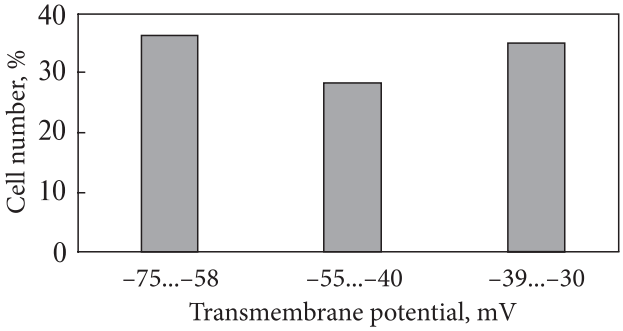

Fig. 8. Distribution of L929 cells by transmembrane potential in suspension after freezing with 5% DMSO

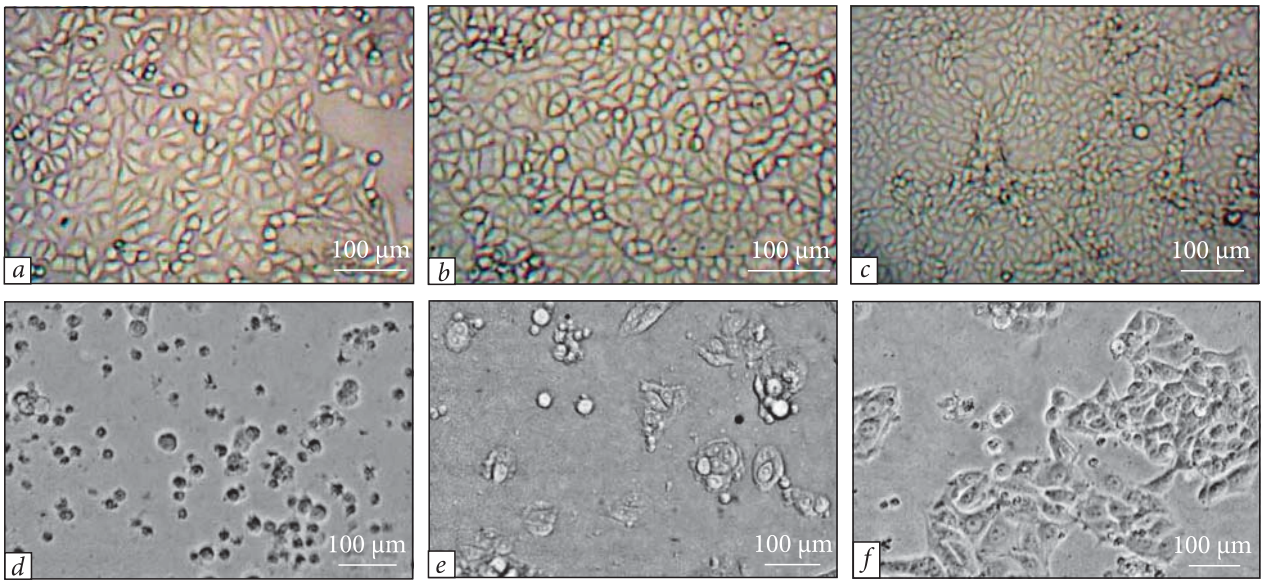

Fig. 9. L929 cells that were adhered to a glass surface after freezing with 10% (*a*, *b*, *c*) and 5% DMSO (*d*, *e*, *f*) depending on the period of attachment to the substrate (*a*, *d* — 1 day; *b*, *e* — 2 days; *c*, *f* — 3 days)

and S-phase cells. These results indicate that V_{mem} in rat MSCs hyperpolarizes during the progression of the cycle from early G1 to S phase. Such fluctuations in V_{mem} are well documented in other cell types [7]. Therefore, V_{mem} oscillation is an important regulatory component of ion flux during the cell cycle, and its dysregulation may be associated with abnormal cell behaviour.

Modulation of V_{mem} can stimulate or inhibit proliferation in predictable ways. When varying the V_{mem} levels of Chinese hamster ovary cells by changing the ionic composition of the medium, complete mitotic arrest was achieved by hyperpolarizing V_{mem} to −75 mV, but its recovery could be obtained by returning to V_{mem} to −10 mV [14]. In rat spinal cord astrocytes, hyperpolarization of the membrane potential (approximately −50 mV to −80 mV) was accompanied by a decrease in proliferation [33]. Conversely, depolarization of astrocytes with ouabain or extracellular K^+ increased cell proliferation and DNA synthesis [10, 40].

However, the relationship between V_{mem} and proliferation is not straightforward. Since V_{mem} is a parameter that reflects the cumulative activity of multiple ion channels and currents, V_{mem}-induced cell behaviour may be the result of one or more ion-related events [1]. Many studies have indicated that K^+ currents are the protagonists of proliferation and cell cycle progression [17, 33]. A correlation between inhibition of K^+-channels and inhibition of proliferation has been shown for different cell types [33, 47]. For example, in neural progenitor cells isolated from adult mouse neurospheres, two types of K^+-channels were responsible for establishing a resting hyperpolarized V_{mem} of approximately –80 mV [48].

X.L. Deng *et al.* [16] showed that in a suspension of MSCs obtained from rat bone marrow, in the control group (cells that were not subjected to special treatment) approximately 51% of the cells were in the G0/G1 phase (V_{mem} ~ −41.3 mV), 43% in the S-phase (~ −52.2 mV) and only 6% in the G2/M phase (~ −26...−15 mV). Thus, the cells in the control suspension are in different phases of the cell cycle, although only a small percentage of them are in the division stage and have a low V_{mem} value (depolarized cells). We obtained a similar result for the control suspension of L929 cells (Table 2). Most cells (82%) are in a hyperpolarized state of varying degrees (G1 and S phases), ~10% in a relatively depolarized state (G0/early G1 phase) and ~7% in a depolarized state (in M phase). After freezing in the optimal mode, 84.5% of cells are in a hyperpolarized state of varying degrees (G1 and S phase) and 14.5% of cells in a relatively depolarized state (G0/early G1 phase). The fraction of cells in a depolarized state, *i.e.* cells that were in the division stage, disappears

The cell suspension after freezing with 5% DMSO contains 36% of cells in a hyperpolarized, 28.5% of cells in a relatively hyperpolarized state, and the fraction of cells in a relatively depolarized state increase sharply (35%). However, given that cells after freezing with 5% DMSO lose their

ability to adhere, it is obvious that in this case it is not worth correlating the distribution of cells by V_{mem} with the stages of the cell cycle. As already noted, V_{mem} is a parameter that reflects the cumulative activity of many ion channels and currents. During freeze-thawing, cells are exposed to various damaging factors. The first candidate for cryodamage is the cell plasma membranes and their surface structures. At the same time, one of the main indicators of plasma membrane damage is a disturbance of its permea-bility to varying degrees. This usually causes an increase in the leakage of cations, and therefore a change in V_{mem}. Thus, V_{mem} is no longer associated only with changes in the activity of specific channels that regulate the transmembrane potential, but is also determined by the degree of plasma membrane damage. For example, it was shown that apoptosis of hLEC cells correlated with suppression of integrin expression, decreased proliferation, and depolarization of V_{mem} [37].

Cell adhesion to the extracellular matrix is essential for normal cell cycle progression and accurate cell division [22, 23, 39]. L.C. McKinney and E.K. Gallin [35] showed on mouse macrophage cells that the specific K_i conductance (G_{Ki}) increased almost twofold one day after plating. V_{mem} also increased from −42 to −58 mV over the same time period (G1 to S phase transition). G_{Ki} and V_{mem} correlated with each other. According to F. Krötz *et al*. [28], epoxyeicosatrienoic acids (EEAs) hyperpolarize platelets and inactivate them by inhibiting the expression of adhesion molecules and platelet adhesion to cultured endothelial cells in a V_{mem}-dependent manner. Flow cytometric measurement of platelet V_{mem} using the fluorescent dye diBA-C4-(3) showed a resting potential of −58 mV. Different regioisomers of EEAs hyperpolarized platelets to −69 mV, which was prevented by the nonspecific potassium channel inhibitor charybdotoxin and the use of the large-conductance calcium-activated potassium channel blocker iberiotoxin. Thus, the cell cycle and cell adhesion are two interdependent processes that mutually regulate each other at each phase of the cell cycle. Cell adhesion to the extracellular matrix via integrin receptors triggers signalling pathways necessary for cell cycle progression [2, 21, 24, 42].

CONCLUSIONS

Methods for determining the absolute values of cell transmembrane potentials using potential-dependent fluorescent probes provide broad opportunities for monitoring transmembrane potentials in suspensions of small cultured cells under the influence of various factors.

The control suspension of L929 cells contains cells in different phases of the cell cycle. The majority of cells (82%) are in a hyperpolarized state of varying degrees (G1 and S phases), and only a small percentage are in the division stage and have a low transmembrane potential (depolarized cells).

Freezing of L929 cell suspension under optimal conditions (10% DMSO, cooling rate of 1 °C/min to −80 °C with subsequent immersion in liquid nitrogen) practically does not change the proportion of cells in the hyperpolarized state. At the same time, the fraction of cells in the depolarized state disappears. Obviously, cells that were in the division stage are more sensitive to cryodamage factors.

Freezing of L929 cell suspension with 5% DMSO using the same cooling regimen resulted in a significant decrease in the proportion of cells in a hyperpolarized state and a significant decrease in the ability of cells to adhere.

Transmembrane potential is a parameter that reflects the cumulative activity of many ion channels and currents. In this case, cell damage during cryopreservation causes a change in the permeability of cell membranes and disrupts the direct connection between V_{mem} and the functioning of specific ion channels. An additional contribution to this imbalance is made by disruption of processes associated with the expression of integrins and other participants in the adhesion process.

REFERENCES

1. Adams DS, Levin M. Strategies and techniques for investigation of biophysical signals in patterning. In: Whitman M, Sater AK, editors. Analysis of growth factor signaling in embryos. Boca Raton: CRC Press; 2006. p. 177—262.
2. Assoian RK, Schwartz MA. Coordinate signaling by integrins and receptor tyrosine kinases in the regulation of G1 phase cell-cycle progression. Curr Opin Genet Dev. 2001; 11(1): 48—53.
3. Ataullakhanov FI, Martinov MV, Shi Q, Vitvitsky VM. Significance of two transmembrane ion gradients for human erythrocyte volume stabilization. PLoS ONE. [Internet]. 2022 Dec 21 [cited 2026 Apr 20]; 17(12): e0272675. Available from: https://journals.plos.org/plosone/article?id=10.1371/journal.pone.0272675
4. Balach MM, Casale CH, Campetelli AN. Erythrocyte plasma membrane potential: past and current methods for its measurement. Biophys Rev. 2019; 11(6):995—1005.
5. Bancila V, Nikonenko I, Dunant Y, Bloc A. Zinc inhibits glutamate release via activation of presynaptic KATP channels and reduces ischaemic damage in rat hippocampus. J Neurochem. 2004; 90(5): 1243—50.
6. Bankers-Fulbright JL, Gleich GJ, Kephart GM, et al. Regulation of eosinophil membrane depolarization during NADPH oxidase. J Cell Sci. 2003; 116(Pt 15): 3221—6.
7. Barghouth PG, Thiruvalluvan M, Oviedo NJ. Bioelectrical regulation of cell cycle and the planarian model system. Biochim Biophys Acta, 2015; 1848(10 Pt B): 2629—37.
8. Binggeli R, Weinstein RC. Membrane potentials and sodium channels: Hypotheses for growth regulation and cancer formation based on changes in sodium channels and gap junctions. J Theor Biol. 1986; 123(4): 377—401.
9. Blackiston DJ, McLaughlin KA, Levin M. Bioelectric controls of cell proliferation: ion channels, membrane voltage and the cell cycle**.** Cell Cycle. 2009; 8(21): 3527—36.
10. Bordey A, Sontheimer H. Postnatal development of ionic currents in rat hippocampal astrocytes in situ. J Neurophysiol. 1997; 78(1): 461—77.
11. Brauner T, Holser DF, Strasser RJ. Comparative measurements of membrane potentials with microelectrodes and voltage-sensitive dyes. Biochim Biophys Acta. 1984; 771(2): 208—16.
12. Chifflet S, Hernandez JA, Grasso S. A possible role for membrane depolarization in epithelial wound healing. Am J Physiol Cell Physiol. 2005; 288(6): 1420—30.
13. Cohen LB, Keynes, RD, Hille B. Light scattering and birefringence changes during nerve activity. Nature. 1968; 218(5149): 438—41.
14. Cone CD Jr., Tongier M Jr. Contact inhibition of division: Involvement of the electrical transmembrane potential. J Cell Physiol, 1973; 82(3): 373—86.
15. Defrise-Quertain F, Fraser-L'Hostis C, Coral D, Deshusses J. Kinetic study of the plasma-membrane potential in procyclic and bloodstream forms of Trypanosoma brucei using the fluorescent probe bisoxonol. Biochem J. 1996; 314(Pt 2): 595—601.
16. Deng XL, Lau CP, Lai K, et al. Cell cycle-dependent expression of potassium channels and cell proliferation in rat mesenchymal stem cells from bone marrow. Cell Prolif. 2007; 40(5): 656—70.
17. Dubois JM, Rouzaire-Dubois B. Role of potassium channels in mitogenesis. Prog Biophys Mol Biol. 1993; 59(1): 1—21.
18. Emri M, Balkay L, Krasznai Z, et al. Wide applicability of a flow cytometric assay to measure absolute membrane potentials on the millivolt scale. Eur Biophys J. 1998; 28: 78—83.
19. Hamill OP, Marty A, Neher E, et al. Improved patch clamp techniques for high-resolution current recording from cells and cell-free membrane patches. Pflugers Arch. 1981; 391(2): 85—100.
20. Hosoi S, Slayman CL. Membrane voltage, resistance, and channel switching in isolated mouse fibroblasts (L cells): a patch-electrode analysis. J Physiol. 1985; 367: 267—90.
21. Jones MC, Askari JA, Humphries JD, Humphries MJ. Cell adhesion is regulated by CDK1 during the cell cycle. J Cell Biol. 2018; 217(9): 3203—18.
22. Jones MJ, Jones MC. Cell cycle control by cell-matrix interactions. Curr Opin Cell Biol. [Internet]. 2023 Dec 5 [cited 2026 Apr 20]; 86: 102288; Available from: https://www.sciencedirect.com/science/article/pii/S0955067423001370
23. Jones MC, Zha J, Humphries MJ**.** Connections between the cell cycle, cell adhesion and the cytoskeleton. Philos Trans R Soc Lond B Biol Sci. [Internet]. 2019 Jul 1 [cited 2026 Apr 20]; 374(1779): 20180227. Available from: https://royalsocietypublishing.org/rstb/article/374/1779/20180227/42314/Connections-between-the-cell-cycle-cell-adhesion
24. Kamranvar SA, Rani B, Johansson S. Cell cycle regulation by integrin-mediated adhesion. Cells. [Internet]. 2022 Aug 14 [cited 2026 Apr 20]; 11(16): 2521. Available from: https://www.mdpi.com/2073-4409/11/16/2521
25. Konig S, Hinard V, Arnaudeau S, et al. Membrane hyperpolarization triggers myogenin and myocyte enhancer factor-2 expression during human myoblast differentiation. J Biol Chem. 2004; 279(27): 28187—96.

26. Kopper KL, Adorante JS. Regulation of intracellular calcium in N1E-115 neuroblastoma cells: The role of Na^+/Ca^{2+} exchange. Am J Physiol Cell Physiol. 2002; 282(5): 1000—8.
27. Krasznai Z, Marian T, Balkay L, et al. Flow cytometric determination of absolute membrane potential of cells. J Photochem Photobiol B: Biol. 1995; 28(1): 93—9.
28. Krötz F, Riexinger T, Buerkle T.M. Membrane-potential-dependent inhibition of platelet adhesion to endothelial cells by epoxyeicosatrienoic acids. Arterioscler Thromb Vasc Biol. 2004; 24(3): 595—600.
29. Langheinrich U, Daut J. Hyperpolarization of isolated capillaries from guinea-pig heart induced by K^+ channel openers and glucose deprivation. J Physiol. 1997; 502(Pt 2): 397—408.
30. Laris PC, Pershadsingh HA, Johnstone RM. Monitoring membrane potentials in Erhlich ascites tumor cells by means of a fluorescent dye. Biochim Biophys Acta, 1976; 436(2): 475—88.
31. Lew VL. The circulatory dynamics of human red blood cell homeostasis: Oxy-deoxy and PIEZO1-triggered changes, Biophys J. 2023; 122(3): 484—95,
32. Li GR, Deng XL, Sun H, et al. Ion channels in mesenchymal stem cells from rat bone marrow. Stem Cells, 2006; 24(6): 1519—28.
33. MacFarlane SN, Sontheimer H. Changes in ion channel expression accompany cell cycle progression of spinal cord astrocytes. GLIA, 2000; 30(1): 39—48.
34. Maric D, Maric I, Smith SV, et al. Potentiometric study of resting potential, contributing K channels and the onset of Na channel excitability in embryonic rat cortical cells. Eur J Neurosci. 1998; 10(8): 2532—46.
35. McKinney LC, Gallin EK. Effect of adherence, cell morphology, and lipopolysaccharide on potassium conductance and passive membrane properties of murine macrophage J774.1 cells. J Membr Biol. 1990; 116(1): 47—56.
36. Mauritz JMA, Seear R, Esposito A, et al. X-Ray microanalysis investigation of the changes in Na, K, and hemoglobin concentration in plasmodium falciparum-infected red blood cells. Biophys J. 2011; 100(6): 1438—45.
37. Nebe B, Kunz F, Peters A, et al. Induction of apoptosis by the calcium antagonist mibefradil correlates with depolarization of the membrane potential and decreased integrin expression in human lens epithelial cells. Graefes Arch Clin Exp Ophthalmol. 2004; 242(7): 597—604.
38. Newell EW, Schlichter LC. Integration of K and Cl currents regulate steady-state and dynamic membrane potentials in cultured rat microglia. J Physiol. 2005; 567(Pt 3): 869—90.
39. Rani B, Gupta DK, Johansson S, Kamranvar SA. Contribution of integrin adhesion to cytokinetic abscission and genomic integrity. Front Cell Dev Biol. [Internet]. 2022 Dec 12 [cited 2026 Apr 20]; 10: 1048717. Available from: https://www.frontiersin.org/journals/cell-and-developmental-biology/articles/10.3389/fcell.2022.1048717/full
40. Ransom CB, Sontheimer H. Biophysical and pharmacological characterization of inwardly rectifying K^+ currents in rat spinal cord astrocytes. J Neurophysiol. 1995; 73(1): 333—46.
41. RevinVV, Gromova NV, Revina ES, at al. Study of the structure, oxygen-transporting functions, and ionic composition of erythrocytes at vascular diseases. Biomed Res Int. [Internet]. 2015 Oct 27 [cited 2026 Apr 20]; 2015: 973973. Available from: https://onlinelibrary.wiley.com/doi/10.1155/2015/973973
42. Schwartz MA, Assoian RK. Integrins and cell proliferation: Regulation of cyclin-dependent kinases via cytoplasmic signaling pathways. J Cell Sci. 2001; 114(Pt 14): 2553—60.
43. Seidl J, Knuechel R, Kunz-Schughart LA. Evaluation of membrane physiology following fluorescence activated or magnetic cell separation. Cytometry, 1999; 36(2): 102—11.
44. Sudsiri CJ, Ritchie RJ. Influence of Na+ disorder on cytoplasmic conductivity and cellular electromagnetic (EM) energy absorption of human erythrocytes. (PONE-D-21-36089). PLOS ONE. [Internet]. 2023 Feb 23 [cited 2026 Apr 20]; 18(2): e0277044. Available from: https://journals.plos.org/plosone/article?id=10.1371/journal.pone.0277044
45. Sundelacruz S, Levin M, Kaplan DL. Role of membrane potential in the regulation of cell proliferation and differentiation. Stem Cell Rev Rep. 2009; 5(3): 231—46.
46. Szaszi K, Sirokmany G, Di Ciano-Oliveira C, et al. Depolarization induces Rho-Rho kinase-mediated myosin light chain phosphorylation in kidney tubular cells. Am J Physiol Cell Physiol. 2005; 289(3): 673—85.
47. Wonderlin WF, Strobl JS. Potassium channels, proliferation and G1 progression. J Membr Biol. 1996; 154(2): 91—107.
48. Yasuda T, Bartlett PF, Adams DJ. K_{ir} and K_v channels regulate electrical properties and proliferation of adult neural precursor cells. Mol Cell Neurosci. 2008; 37(2): 284—97.

Received 17.01.2026
Accepted for publication 18.05.2026

О.І. Гордієнко, Є.І. Смольянінова, Г.Л. Полякова,*
С.Є. Коваленко, І.Ф. Коваленко, О.Ф. Тодрін
Інститут проблем кріобіології і кріомедицини НАН України,
м. Харків Україна
*olga.gordiyenko.ipcic@gmail.com

РОЗПОДІЛ КЛІТИН L929 ЗА ТРАНСМЕМБРАННИМ ПОТЕНЦІАЛОМ
У СУСПЕНЗІЇ ДО ТА ПІСЛЯ ЗАМОРОЖУВАННЯ

У роботі визначено розподіл за трансмембранним потенціалом клітин L929 у культивованій суспензії та після заморожування. Показано, що у контрольній суспензії клітини знаходяться у різних фазах клітинного циклу: більша частка клітин (82 %) — у гіперполяризованому стані різного ступеню (G1 та S-фази), і лише незначна їх частка (~7 %) перебуває у стадії поділу та має низьке значення трансмембранного потенціалу (деполяризовані клітини). Заморожування суспензії клітин L929 за стандартним протоколом (10% ДМСО, швидкість охолодження 1 °С/хв до –80 °С із подальшим зануренням у рідкий азот) практично не змінює частку клітин у гіперполяризованому стані. Водночас зникає фракція клітин у деполяризованому стані. Очевидно, що клітини, які перебувають у стадії поділу, є більш чутливими до кріопошкодження. Заморожування суспензії клітин L929 зі зниженою концентрацією ДМСО (5%) призводить до значного зменшення частки клітин у гіперполяризованому стані та суттєвого зменшення їхньої здатності до адгезії.

***Ключові слова*:** клітини L929, трансмембранний потенціал, клітинний цикл, адгезія, заморожування.